Applied Physics Letters

Enhanced extreme ultraviolet high-harmonic generation from chromium-doped magnesium oxide

Cite as: Appl. Phys. Lett. **118**, 201103 (2021); https://doi.org/10.1063/5.0047421
Submitted: 13 February 2021 . Accepted: 13 April 2021 . Published Online: 17 May 2021

V. E. Nefedova, S. Fröhlich, F. Navarrete, N. Tancogne-Dejean, D. Franz, A. Hamdou, S. Kaassamani, D. Gauthier, R. Nicolas, G. Jargot, M. Hanna, P. Georges, M. F. Ciappina, U. Thumm, W. Boutu, and H. Merdji

Applied Physics Letters ARTICLE scitation.org/journal/apl

Enhanced extreme ultraviolet high-harmonic generation from chromium-doped magnesium oxide

Cite as: Appl. Phys. Lett. **118**, 201103 (2021); doi: 10.1063/5.0047421
Submitted: 13 February 2021 · Accepted: 13 April 2021 ·
Published Online: 17 May 2021

V. E. Nefedova,[1] S. Fröhlich,[1] F. Navarrete,[2,3] N. Tancogne-Dejean,[4] D. Franz,[1] A. Hamdou,[1] S. Kaassamani,[1] D. Gauthier,[1] R. Nicolas,[1,5] G. Jargot,[6,7] M. Hanna,[6] P. Georges,[6] M. F. Ciappina,[8,9,10] U. Thumm,[2,a)] W. Boutu,[1] and H. Merdji[1,a)]

AFFILIATIONS

[1]Ultrafast Nanophotonics Group, LIDYL, CEA-CNRS-Université Paris-Saclay, 91191 Gif-sur-Yvette, France
[2]Department of Physics, Kansas State University, Manhattan, Kansas 66506, USA
[3]Institute of Physics, University of Rostock, 18051 Rostock, Germany
[4]Max Planck Institute for the Structure and Dynamics of Matter and Center for Free-Electron Laser Science, Luruper Chaussee 149, 22761 Hamburg, Germany
[5]Department of Natural Sciences, Lebanese American University, 1102 Beirut, Lebanon
[6]Université Paris-Saclay, Institut d'Optique Graduate School, CNRS, Laboratoire Charles Fabry, 91127 Palaiseau, France
[7]Fastlite, Sophia Antipolis, 06600 Antibes, France
[8]ICFO-Institut de Ciences Fotoniques, The Barcelona Institute of Science and Technology, Avenue Carl Friedrich Gauss 3, 08860 Castelldefels (Barcelona), Spain
[9]Physics Program, Guangdong Technion–Israel Institute of Technology, Shantou, Guangdong 515063, China
[10]Technion–Israel Institute of Technology, Haifa 32000, Israel

[a)]**Authors to whom correspondence should be addressed**: thumm@phys.ksu.edu and hamed.merdji@cea.fr

ABSTRACT

High-order harmonic generation (HHG) from crystals is emerging as a new ultrashort source of coherent extreme ultraviolet (XUV) light. Doping the crystal structure can offer a new way to control the source properties. Here, we present a study of HHG enhancement in the XUV spectral region from an ionic crystal, using dopant-induced vacancy defects, driven by a laser centered at a wavelength of 1.55 μm. Our numerical simulations based on solutions of the semiconductor Bloch equations and density-functional theory are supported by our experimental observations and demonstrate an increase in the XUV high harmonic yield from doped bulk magnesium oxide (MgO) compared to undoped MgO, even at a low defect concentration. The anisotropy of the harmonic emission as a function of the laser polarization shows that the pristine crystal's symmetry is preserved. Our study paves the way toward the control of HHG in solids with complex defects caused by transition-metal doping.

The interaction of an electric field in the strong-field regime with a semiconductor or a dielectric generates electron–hole pairs, which are subsequently accelerated by this field and emit coherent radiation via inter- and intra-band electronic transitions in the solid.[1–4] This coherent emission occurs as bursts of attosecond pulses that have been observed as a harmonic comb in the frequency domain. Since its first experimental observation,[5] considerable efforts were devoted to the understanding of the main mechanisms behind high-order harmonic generation in solids (HHG). This new source of extreme ultraviolet (XUV) radiation[6,7] displays a high degree of coherence,[8] for instance, suitable for lensless diffractive imaging.[9] It recently provided beams carrying orbital angular momentum with a selective topological charge.[10] Recent studies also reveal that the HHG spatiotemporal properties are intricate due to the complex light-driven electronic

dynamics inside the solid. Hence, as a basic application, HHG can reveal information about the crystal's electronic band structure and intrinsic crystal properties.[4,11] Future applications will exploit the ability to manipulate the light-driven electron motion during the crystal HHG process to create optoelectronic devices operating at petahertz frequencies[12–14] or to extract topological information.[15] However, increasing the yield is a prerequisite for the development of a solid-state HHG source and its applications. Various experimental techniques, such as plasmon-,[16,17] waveguide-,[9,18,19] and antenna-enhanced HHG,[20] were already implemented to achieve this goal. Here, we propose an alternative way of boosting the HHG yield from solids based on defects. This approach exploits the modification and control of the active medium's electronic structure to tailor the high-order harmonic output signal. Since defects are a cornerstone of most modern electronic devices, it appears promising to investigate their influence on the HHG yield. The addition of dopants creates electronic states in the bandgap, leading to modifications of the electronic band structure[21,22] and bandgaps,[23–26] allowing additional optical transitions.[27] Another significant effect of doping is the appearance of point defects such as vacancies and interstitial sites.[28,29] According to recent theoretical investigations, dopant-induced bandgap changes can substantially influence the HHG process.[29–33] In particular, donor-doped materials were theoretically predicted to enhance the HHG yield due to electronic excitation from impurity states.[31,33]

We here investigate the influence of dopant-induced vacancies on the HHG yield in chromium-doped magnesium oxide (MgO:Cr), which was extensively studied previously using experimental[34–37] and numerical[38–40] methods. The Cr donor-dopants were found not only to substitute atoms with Cr^{3+} ions in the MgO lattice providing additional electrons but also to cause the formation of vacancies[34–37] in order to maintain charge neutrality.[37]

The HHG process in gases is well explained by the semi-classical "three-step model."[41–43] A similar approach has been proposed in crystals, where a strong laser electric field generates electron–hole pairs, which are subsequently accelerated by this field and emit radiation via inter- and intra-band opto-electronic transitions in the solid.[1–4] The competition between those two mechanisms depends on the material. As a general feature, the driving laser parameters and, as a general feature, intra-band emission dominate at lower and inter-band emission at higher HHG photon energies, the latter including the plateau and cutoff domain of the HHG spectrum.

Figure 1 presents a scheme of the basic mechanisms involved in the HHG process in pristine and doped MgO. Here, the Cr donor-dopants not only substitute Mg atoms with Cr^{3+} ions in the MgO lattice, providing additional electrons [see Figs. 1(a) and 1(b)] but also cause the formation of vacancies[34–37] to maintain charge neutrality.[37] The underlying electronic excitations in pristine and Cr-doped MgO are sketched in Figs. 1(c) and 1(d), respectively. An electron wave packet is (1) excited from the valence band (VB) to the first conduction band (CB1) with an initial field-dressed crystal momentum at the minimum bandgap (referred to as the $\Gamma-$ point), where it (2) experiences intra-band acceleration. In case the laser electric field is strong enough, an electron wave packet is excited to a higher conduction band (CB2), where intra-band acceleration occurs, before (3) de-exciting to the VB upon recombination with its residual hole, emitting harmonics with photon energies equal to the instantaneous gap in the first BZ.

Within the Keldysh model for strong-field ionization[44] and a saddle-point analysis,[45,46] a closed-form semi-quantitative approximation for the above bandgap (inter-band transition) yield is given by[47,48]

$$Y_{\mathrm{MgO}}(E) \propto \exp\left[-\frac{\sqrt{8\, m^*_{vb-cb1}}\, \varepsilon_g^{3/2}}{e\hbar E}\right], \tag{1}$$

where $m^*_{vb-cb1} = (|\frac{1}{m^*_{vb}}| + |\frac{1}{m^*_{cb1}}|)^{-1}$ is the reduced effective mass of the VB and CB1, given in terms of their respective effective masses, m^*_{vb} and m^*_{cb1}, ε_g is the minimum bandgap energy between VB and CB1, and E is the peak field strength of the driving laser pulse. Similarly, we can account for excitations to higher conduction bands, e.g., to CB2 in our calculations, as sketched in Figs. 1(c) and 1(d), leading to the emission of harmonics at higher frequencies upon recombination to the VB. For a fixed driving electric-field amplitude, Eq. (1) predicts that a decrease in the minimum bandgap or reduced effective mass increases the HHG spectral yield above the minimum bandgap. Note that the effective electron mass is a crucial parameter, responsible for the electron mobility in solids. Its energy-dependent behavior was recently investigated.[49,50] Since the Cr impurities with associated vacancies break the transitional symmetry of the MgO crystal (in the BZ of the pristine crystal), impurity levels couple with states of the valence and conduction bands along the entire BZ. Together with the dispersion-free-electron nature of MgO impurity levels,[29,51,52] which implies a very large effective mass, the loss of symmetry allows us to represent impurity levels as flatbands in the BZ of the pristine sample [shown as extended horizontal lines in Figs. 1(c) and 1(d)]. The impurity-defect band (IDB) appears close to the CB1, and the vacancy defect band (VDB) emerges close to the VB. Adapting Eq. (1) to transitions from the VDB in MgO:Cr, we obtain the estimate for VDB contributions to the HHG yield

$$Y_{\mathrm{MgO:Cr}}(E) \propto \exp\left[-\frac{\sqrt{8\, m^*_{vdb-cb1}}\, (\varepsilon_{cb1} - \varepsilon_{vdb})^{3/2}}{e\hbar E}\right], \tag{2}$$

where $m^*_{vdb-cb1}$ is the reduced effective mass between CB1 and VDB. Because of the large VDB effective mass, we can approximate $m^*_{vdb-cb1} \approx m^*_{cb1} > m^*_{vb-cb1}$. Thus, the reduced effective mass is greater than that for the pristine sample. Nevertheless, because of the reduction of the bandgap induced by the vacancy, the numerator of the exponential in Eq. (2) is smaller than in Eq. (1), suggesting an enhancement of the HHG yield due to symmetry-allowed VDB–CB1 optical transitions.

For a fully quantitative description of HHG from pristine and doped MgO, we numerically solve the semiconductor Bloch equations (SBEs), including the VB, IDB, CB1, and CB2 (for details, see supplementary material SI.3). Disregarding temperature effects, the Fermi energy of MgO:Cr lies approximately between VDB and CB1,[53] so that the VB and VDB are initially occupied.

Figures 2(a) and 2(b) show the calculated HHG spectra from MgO and MgO:Cr, respectively. Both spectra are composed of odd harmonics (except for a dim even harmonic for the calculated spectra from MgO:Cr) and exhibit almost the same field-strength dependence of the cutoff. The main difference between them is the increased inter-band harmonic spectral yield at above-bandgap photon energies for the material with vacancy defects. We analyze the HHG-yield

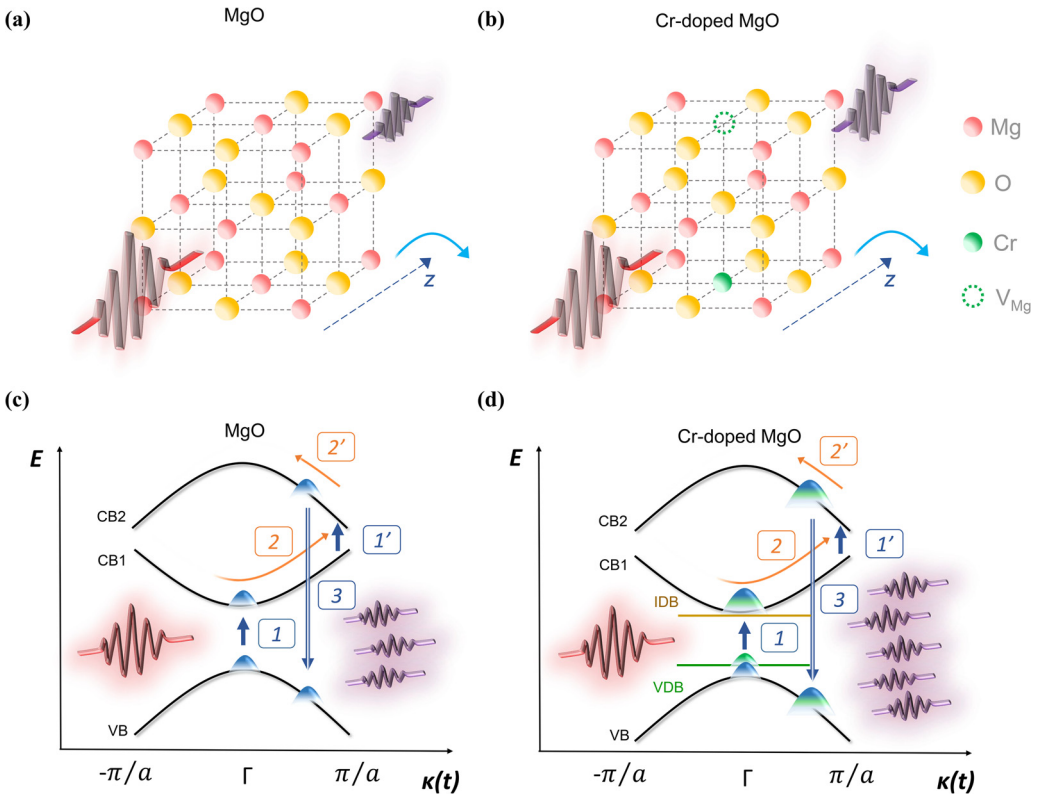

FIG. 1. Schematic of HHG in (a) and (c) MgO and (b) and (d) MgO:Cr in (a) and (b) coordinate and (c) and (d) momentum space. In (a) and (b), the laser propagation axis is indicated as z, around which crystals are rotated (light blue arrow) during anisotropy measurements [cf. Figs. 4(a) and 4(b)]. (b) A Mg vacancy replaces the closest Mg^{2+} ion along the [100] (C_{4v} symmetry) or [110] direction (C_{2v} symmetry). Both C_{4v} and C_{2v} centers are observed experimentally.[27,34] (c) and (d) The laser electric field excites an electron wave packet from the valence band (VB) to the first conduction band (CB1) (1, blue arrow), where it experiences intra-band acceleration (2, orange arrow). At higher driver intensities, excitation to (1′, blue arrow) and acceleration in (2′, orange arrow) higher conductions bands (here CB2) can occur. The excited electron wave packet de-excites to the VB upon recombination with its residual hole (3, blue arrow), emitting harmonics of energy equal to the instantaneous gap in the first BZ. (d) In MgO:Cr, the occupied impurity defect band (IDB) and vacancy defect band (VDB) account for additional electronic transitions that enhance the net high-harmonic yield relative to MgO.

enhancement by comparing the spectra in Figs. 2(a) and 2(b) with our experimental data, estimating the intensity of the driving electric field inside the solids as detailed in the supplementary material SI.7. Our laser field is sufficiently strong to excite electrons to the CB2, leading to the emission of harmonics in the XUV spectral range. Note that the consistent modeling of macroscopic optical effects, and the driving-laser field strength in matter, would require merging our theoretical model with Maxwell's equations, which is beyond the scope of the

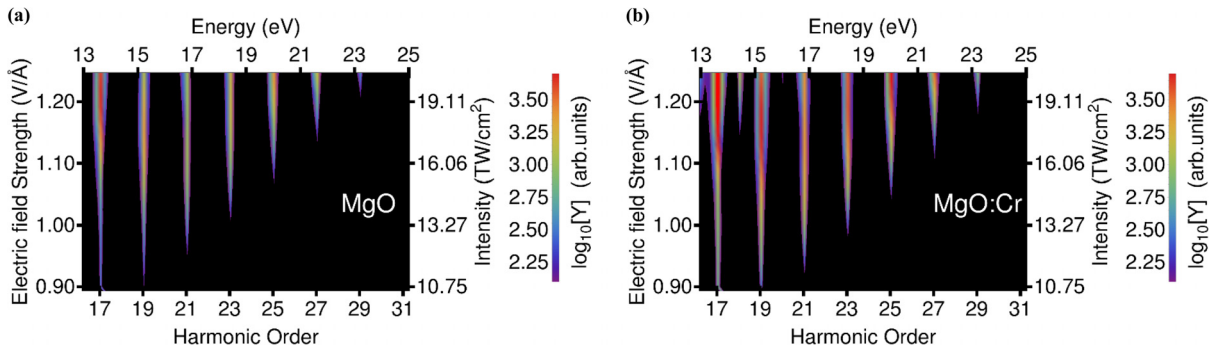

FIG. 2. Calculated HHG spectra from (a) MgO and (b) MgO:Cr crystals for driving laser-pulse incidence and HHG emission in $\Gamma - X$ direction as a function of the driver peak field strength. The laser central wavelength is 1.55 μm (corresponding to a photon energy of 0.80 eV, for details on the experimental parameters, see the supplementary material SI.5). Although the HHG yield from MgO:Cr is larger, we do not find evidence for a HHG cutoff extension for the doped sample.

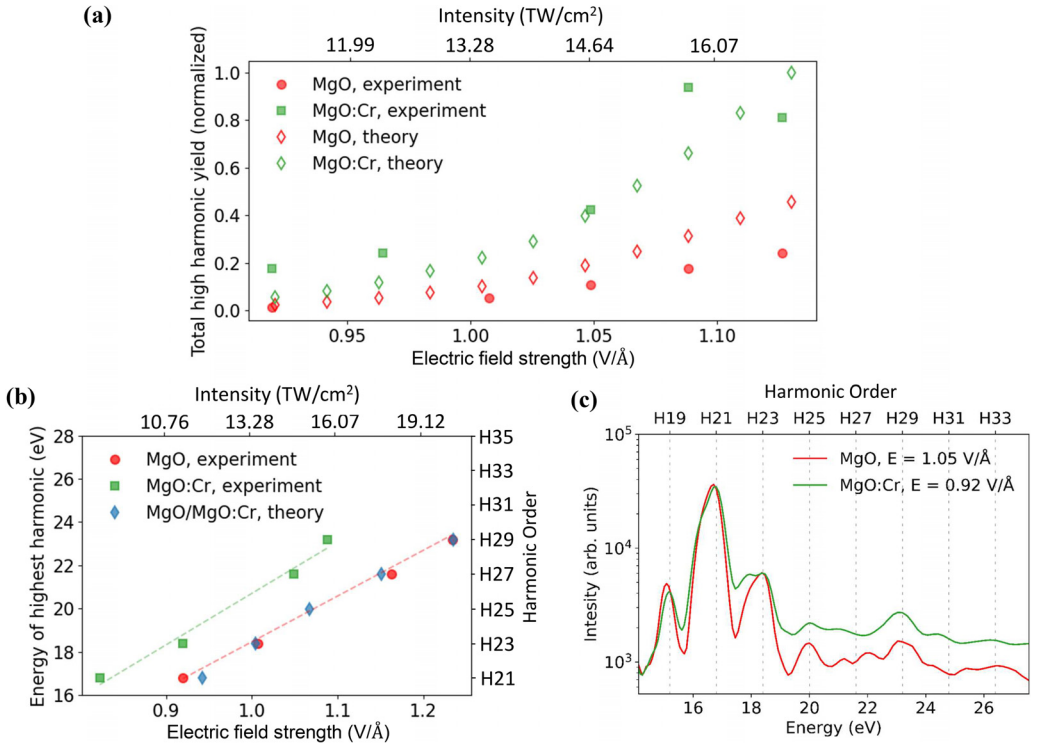

FIG. 3. Comparison of HHG signals from MgO and MgO:Cr crystals for a driving laser central wavelength of 1.55 μm (corresponding to a photon energy of 0.80 eV), (a) measured and calculated total harmonic yields in the $\Gamma - X$ direction, integrated over photon energies between 14.4 and 25.6 eV, as a function of the peak driving laser-electric-field strength. The integrated HHG yield from MgO:Cr crystal is larger. (b) Highest observable harmonic energy vs the driving field strength in the $\Gamma - X$ direction. The offset of the observed highest harmonic in both spectra is about 2 eV over a broad range of laser-electric-field strengths. It approximately matches the bandgap-energy difference between doped and undoped crystals. Dashed and solid lines are linear interpolations added to guide the eye. (c) Experimental HHG spectra obtained from MgO at a vacuum laser field strength of 1.05 V/Å (14.6 TW/cm^2) and from MgO:Cr at a vacuum laser field strength of 0.92 V/Å (11.2 TW/cm^2). In MgO:Cr, a weaker laser electric field results in a comparable integrated HHG yield.

current manuscript. Spectral transmission aspects are addressed in supplementary material SI.2. The setup, intensity estimation, and the detailed description of the samples are given as supplementary material. Both crystals, MgO and MgO:Cr, are 200-μm-thick with (001) oriented surfaces. We confirm the presence of Cr^{3+} ions in the MgO:Cr sample by photoluminescence measurements (supplementary material SI.1). In addition, the calculated densities of states (DOS) for MgO and MgO:Cr reveal defect states above the topmost valence band in MgO:Cr (supplementary material SI.4). Our transmission measurements show a bandgap-energy reduction of 1.8 eV in MgO:Cr, compared to the pure MgO bandgap energy of 7.16 eV (supplementary material SI.2).

Figure 3(a) shows the dependence of the experimental harmonic yield, integrated between 14.4 and 25.6 eV, on the driving laser electric-field strength. The total HHG yield from MgO:Cr is found to be larger than the one of pure MgO, up to a laser-field strength of about 1.15 V/Å (corresponding to an intensity of 18 TW/cm^2). Operating at a repetition rate of 125 kHz, the damage threshold is reached at a laser electric-field strength of 1.23 V/Å (20 TW/cm^2) and 1.09 V/Å (15.7 TW/cm^2) for pure MgO and MgO:Cr, respectively. The lower damage threshold of MgO:Cr is probably associated with the increased electron density. In comparison, Fig. 3(a) presents the numerically calculated intensities of odd harmonics for MgO and MgO:Cr, integrated over the same energy range. Our simulation results show good agreement with the experiment for pristine MgO and two discrepancies for doped MgO: (i) the experimental data show high harmonic emission starting at much lower laser-field strength, 0.71 V/Å (6.74 TW/cm^2), with a smaller slope than that obtained from the simulations based on the solution of SBEs for doped MgO, (ii) the saturation of the HHG emission from MgO:Cr observed in the experiment is not reproduced by theory, since it involves mechanisms, such as radiation damage, which are not taken into account in the simulation. In spite of this, both measured and calculated results exhibit a pronounced increase in the HHG spectral intensity from the MgO:Cr crystal, as the result of added transitions from the VDB.

Figure 3(b) shows the highest harmonic order we are able to detect for driving-laser-field strengths (in vacuum) between 0.82 V/Å (9 TW/cm^2) and 1.23 V/Å (20 TW/cm^2) for both samples. It also shows HHG cutoffs retrieved from our calculated spectra in Figs. 2(a) and 2(b). Figure 3(b) shows a linear scaling of the highest experimentally detected harmonic as a function of the peak-electric-field strength in both MgO and MgO:Cr, with almost the same slope but an energy offset of approximately 2 eV. This energy offset is close to the bandgap-energy difference between MgO and MgO:Cr of $\approx$ 1.8 eV

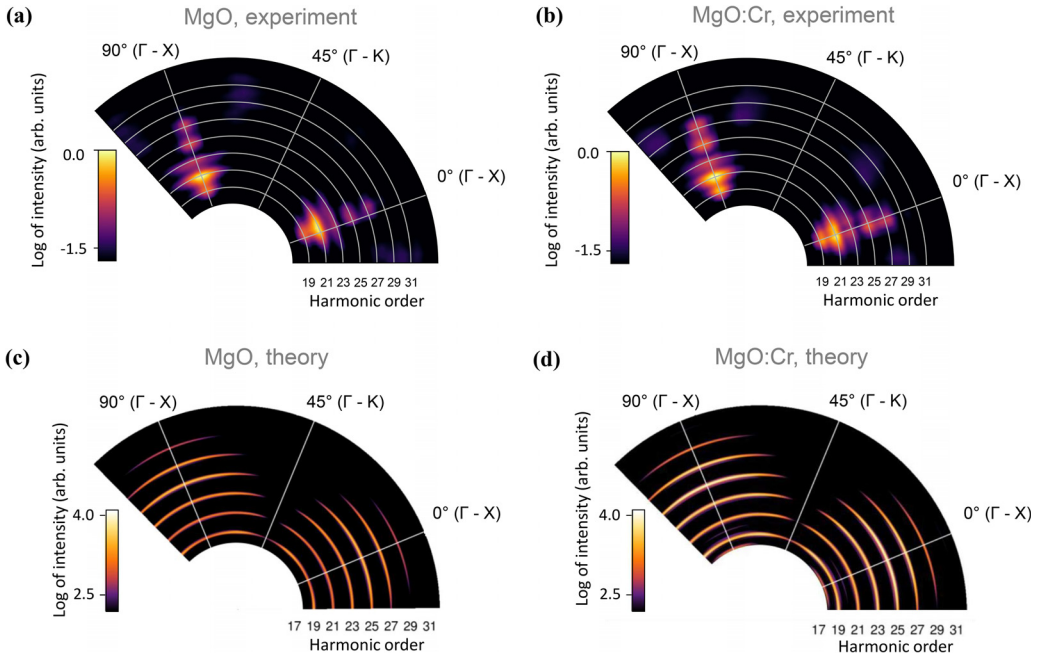

FIG. 4. Crystal-orientation dependence of HHG in (a) and (c) MgO and (b) and (d) MgO:Cr crystals. The crystals are rotated about the laser propagation axis [z axes in Figs. 1(a) and 1(b)] in 3° steps, whereas the linear laser polarization is kept fixed. Measured HHG spectra for (a) MgO at a peak laser-field strength (vacuum value) of 1.23 V/Å (20 TW/cm^2) and (b) MgO:Cr at 1.09 V/Å (15.7 TW/cm^2). Due to the low doping concentration (0.5%), the fourfold symmetry of the MgO cubic crystal structure is unaltered in MgO:Cr. Calculated spectra at 1.23 V/Å for (c) MgO and (d) MgO:Cr.

that we experimentally determined independently using optical transmission measurements (supplementary material SI.2). The highest harmonic order obtained from the simulations in Figs. 2(a) and 2(b) is identical for MgO and MgO:Cr crystals. The extension of the highest experimentally observable harmonic from MgO:Cr is not obvious. Indeed, since for the same electric-field strength the electron wave packet explores the same region of the first BZ of the MgO and MgO:Cr crystals, one might expect identical HHG cutoffs. We attribute the measured apparent extension of the HHG spectra from MgO:Cr to a higher yield in the plateau region. To further illustrate the HHG behavior, Fig. 3(c) displays HHG spectra measured at a driving-laser peak field strength of 0.92 V/Å (11.2 TW/cm^2) for MgO:Cr and of 1.05 V/Å (14.6 TW/cm^2) for MgO. The two spectra have comparable yields even though the HHG spectrum from MgO:Cr was obtained at a lower laser field strength. This is in qualitative agreement with the simulated spectra displayed in Fig. 2. In addition, we notice in the experimental spectra that harmonics above 19 eV are less intense than those below this energy. This sharp transition between these two plateaus has been reported as a contribution from higher conduction bands associated with low population transfer.[54,55]

Moreover, we consider the contribution of macroscopic effects. The driving laser propagation inside the crystal can play a significant role on its initial spatial or spectral properties and the emitted harmonic radiation.[56] Although the optical propagation effects related to the change of linear and nonlinear refractive indices due to doping are unlikely to play a significant role on the driving laser properties in our experiment, given the low dopant concentration of 0.5%,[57–60] we observe the difference of spatial and spectral properties of the harmonic beam from MgO and MgO:Cr. We detect a blueshift of the HHG spectra in MgO:Cr compared to HHG spectra from MgO at a fixed laser intensity (supplementary material SI.5). We associate this wavelength shift to the increased electron density participating in HHG from MgO:Cr. Since the plasma refractive index variation acts as a diverging lens in the spatial domain, we attribute the observed blueshift to plasma-induced defocusing of the fundamental beam (Refs. 61–63 and references therein). Further investigations in a loose geometry configuration or in reflection geometry would limit possible contributions of macroscopic effects.[56] In a more general context, other crystals and/or higher doping rates may induce larger macroscopic aspects, which may play a significant role in enhancement or in spectral or spatial modifications of the HHG properties.[19]

Next, we study the crystal-orientation-dependent HHG response of both crystals. To investigate the HHG anisotropy, we measure the HHG signal as a function of the crystal orientation with respect to the laser polarization, as sketched in Figs. 1(a) and 1(b) and described in supplementary material SI.5. Figures 4(a) and 4(b) present angle-dependent-measured HHG spectra from MgO and MgO:Cr, recorded at their respective optimal conditions for the highest HHG yields, i.e., just below the damage threshold at peak electric-field strengths of 1.23 V/Å (20 TW/cm^2) for MgO and 1.09 V/Å (15.7 TW/cm^2) for MgO:Cr. The fourfold symmetry reflects the face-centered cubic crystal structure of MgO.[64] The HHG yield is largest along the $\Gamma - X$ direction, while no signal is observed along the $\Gamma - K$ direction. Overall, the two anisotropy dependences are comparable, which is consistent with the fact that the crystal symmetry is preserved for our

low dopant concentrations. We observe that, similar to Fig. 3(a), the harmonics emitted from MgO:Cr have a comparable yield at lower driving-field intensities than harmonics from pure MgO. To analyze this behavior, we have calculated the angle-dependent HHG yield for MgO and MgO:Cr at the same peak vacuum electric-field strength of 1.23 V/Å (20 TW/cm^2), as shown in Figs. 4(c) and 4(d). These calculations are performed in reduced dimensionality, representing the crystal as a 2D square lattice using the same model electronic potential as in recent works,[2,65,66] $V(x, y) = V_0 \cos(ax) + V_0 \cos(ay)$, but allowing for a modified oscillation amplitude V_0 at the defect sites in MgO:Cr[30,31,33,67,68] (supplementary material SI.3). Even though the angular spread of the harmonics differs between theory and experiment, we reproduce the maximal yields measured along the $\Gamma - X$ and the minimal yields along the $\Gamma - K$ direction. For all crystal orientations, our numerical simulation predicts a larger HHG yield for MgO:Cr. These two last characteristics are in good qualitative agreement with the present experimental findings.

In conclusion, we present the HHG yield enhancement from MgO doped with chromium atoms compared to a pure MgO crystal. We associate the extension of the highest observable harmonic in MgO:Cr to an increase in the HHG plateau intensity. The HHG-yield increase from the doped crystal is interpreted as optical excitations introduced by occupied defect states in MgO:Cr that arise from Cr^{3+} dopant ions and Mg-vacancy formation in the MgO lattice. This finding is in agreement with our numerical simulations and previous theoretical predictions of enhanced HHG in doped samples.[30,31,33,67] The HHG anisotropy shows that the pristine MgO crystal symmetry is preserved upon doping. Our numerical results do not reproduce the experimentally observed HHG spectral blue shift and saturation, both caused by additional free electrons in the doped MgO, which we attribute to our incomplete description of the driving laser pulse in the solid. Other crystals involved in the HHG or other dopant concentrations may enhance macroscopic effects that could be exploited to boost the HHG yield in specific spectral ranges. As a perspective, our study promotes the development of efficient compact XUV light sources based on doping. Moreover, it has been suggested that HHG from crystals with defects can provide a way to study dipole moments and wave functions of impurity arrangements[68] and, thus, potentially serve as a tomographic measurement of impurity orbitals. Other future studies will concentrate on HHG spectroscopy to extract information on the intrinsic properties of light-driven attosecond electron transport.[69] This would create attractive perspectives toward the development of all-solid-state attosecond sources and petahertz electronics.[12–14,29–33,55]

See the supplementary material for the details on the photoluminescence measurements and optical characterization and properties of pristine and chromium-doped MgO; on the detailed description of the theoretical model for HHG in solids with vacancy defects as well as the appearance of vacancy-induced defect states in MgO:Cr from density functional theory; on the description of experimental setup and comparison of the obtained HHG spectra; and on OPCPA laser system as well as on laser intensity estimation and notation.

The authors thank M. Billon for technical support. We acknowledge support from the PETACom (Petahertz Optoelectronics Communication) FET Open H2020 Grant No. 829153, OPTOLogic (Optical Topologic Logic) FET Open H2020 Grant No. 899794, support from the French ANR through the grant PACHA (No. ANR-17-CE30-0008-01) and the labex PALM (No. ANR-10-LABX-0039-PALM), support the DGA RAPID grant "SWIM." We acknowledge the financial support from the French ASTRE program through the "NanoLight" grant, the Spanish Ministry MINECO (National Plan 15 grant: FISICATEAMO No. FIS2016-79508-P, SEVERO OCHOA No. SEV-2015-0522, FPI), European Social Fund, Fundació Cellex, Fundació Mir-Puig, Generalitat de Catalunya (AGAUR Grant No. 2017 SGR 1341, CERCA/Program), ERC AdG NOQIA, EU FEDER, European Union Regional Development Fund-ERDF Operational Program of Catalonia 2014–2020 (Operation Code: IU16-011424), MINECO-EU QUANTERA MAQS [funded by The State Research Agency (AEI) No. PCI2019-111828-2/10.13039/501100011033], and the National Science Centre, Poland-Symfonia Grant No. 2016/20/W/ST4/00314. F.N. and U.T. acknowledge support from Air Force Office of Scientific Research under Award No. FA9550-17-1-0369 and NSF Grant No. 1802085 (theory for photoemission from surfaces). Any opinions, finding, and conclusions or recommendations expressed in this material are those of the authors and do not necessarily reflect the views of the United States Air Force. U.T. acknowledges partial support from the Chemical Sciences, Geosciences, and Biosciences Division, Office of Basic Energy Sciences, Office of Science, US Department of Energy under Award No. DEFG02-86ER13491. N.T.-D. thanks A. Rubio.

DATA AVAILABILITY

The data that support the findings of this study are available within the article and its supplementary material.

REFERENCES

[1]S. Ghimire, A. D. DiChiara, E. Sistrunk, G. Ndabashimiye, U. B. Szafruga, A. Mohammad, P. Agostini, L. F. DiMauro, and D. A. Reis, "Generation and propagation of high-order harmonics in crystals," Phys. Rev. A **85**, 043836 (2012).
[2]G. Vampa, C. R. McDonald, G. Orlando, D. D. Klug, P. B. Corkum, and T. Brabec, "Theoretical analysis of high-harmonic generation in solids," Phys. Rev. Lett. **113**, 073901 (2014).
[3]T. T. Luu and H. J. Wörner, "High-order harmonic generation in solids: A unifying approach," Phys. Rev. B **94**, 115164 (2016).
[4]N. Tancogne-Dejean, O. D. Mücke, F. X. Kärtner, and A. Rubio, "Impact of the electronic band structure in high-harmonic generation spectra of solids," Phys. Rev. Lett. **118**, 087403 (2017).
[5]S. Ghimire, A. D. DiChiara, E. Sistrunk, P. Agostini, L. F. DiMauro, and D. A. Reis, "Observation of high-order harmonic generation in a bulk crystal," Nat. Phys. **7**, 138 (2011).
[6]G. Vampa, C. McDonald, A. Fraser, and T. Brabec, "High-harmonic generation in solids: Bridging the gap between attosecond science and condensed matter physics," IEEE J. Sel. Top. Quantum Electron. **21**, 8700110 (2015).
[7]M. Garg, M. Zhan, T. T. Luu, H. Lakhotia, T. Klostermann, A. Guggenmos, and E. Goulielmakis, "Multi-petahertz electronic metrology," Nature **538**, 359 (2016).
[8]H. Kim, S. Han, Y. W. Kim, S. Kim, and S.-W. Kim, "Generation of coherent extreme-ultraviolet radiation from bulk sapphire crystal," ACS Photonics **4**, 1627 (2017).
[9]D. Franz, S. Kaassamani, D. Gauthier, R. Nicolas, M. Kholodtsova, L. Douillard, J.-T. Gomes, L. Lavoute, D. Gaponov, N. Ducros, S. Février, J. Biegert, L. Shi, M. Kovačev, W. Boutu, and H. Merdji, "All semiconductor enhanced high-harmonic generation from a single nanostructured cone," Sci. Rep. **9**, 5663 (2019).

[10]D. Gauthier, S. Kaassamani, D. Franz, R. Nicolas, J.-T. Gomes, L. Lavoute, D. Gaponov, S. Février, G. Jargot, M. Hanna, W. Boutu, and H. Merdji, "Orbital angular momentum from semiconductor high-order harmonics," Opt. Lett. **44**, 546 (2019).
[11]A. A. Lanin, E. A. Stepanov, A. B. Fedotov, and A. M. Zheltikov, "Mapping the electron band structure by intraband high-harmonic generation in solids," Optica **4**, 516 (2017).
[12]F. Krausz and M. I. Stockman, "Attosecond metrology: From electron capture to future signal processing," Nat. Photonics **8**, 205 (2014).
[13]J. Schoetz, Z. Wang, E. Pisanty, M. Lewenstein, M. F. Kling, and M. F. Ciappina, "Perspective on petahertz electronics and attosecond nanoscopy," ACS Photonics **6**, 3057 (2019).
[14]S. Sederberg, D. Zimin, S. Keiber, F. Siegrist, M. S. Wismer, V. S. Yakovlev, I. Floss, C. Lemell, J. Burgdörfer, M. Schultze, F. Krausz, and N. Karpowicz, "Attosecond optoelectronic field measurement in solids," Nat. Commun. **11**, 430 (2020).
[15]R. E. F. Silva, A. Jiménez-Galán, B. Amorim, O. Smirnova, and M. Ivanov, "Topological strong-field physics on sub-laser-cycle timescale," Nat. Photonics **13**, 849 (2019).
[16]S. Han, H. Kim, Y.-W. Kim, Y.-J. Kim, S. Kim, I.-Y. Park, and S.-W. Kim, "High-harmonic generation by field enhanced femtosecond pulses in metal-sapphire nanostructure," Nat. Commun. **7**, 13105 (2016).
[17]G. Vampa, B. G. Ghamsari, S. Siadat Mousavi, T. J. Hammond, A. Olivieri, E. Lisicka-Skrek, A. Y. Naumov, D. M. Villeneuve, A. Staudte, P. Berini, and P. B. Corkum, "Plasmon-enhanced high-harmonic generation from silicon," Nat. Phys. **13**, 659 (2017).
[18]D. Franz, R. Nicolas, W. Boutu, L. Shi, Q. Ripault, M. Kholodtsova, B. Iwan, U. E. Etxano, M. Kovacev, J. Biegert, and H. Merdji, "Amplification of high harmonics in 3d semiconductor waveguides," arXiv:09153v1 (2017).
[19]M. Sivis, M. Taucer, G. Vampa, K. Johnston, A. Staudte, A. Naumov, D. Villeneuve, C. Ropers, and P. Corkum, "Tailored semiconductors for high-harmonic optoelectronics," Science **357**, 303 (2017).
[20]K. Imasaka, T. Kaji, T. Shimura, and S. Ashihara, "Antenna-enhanced high harmonic generation in a wide-bandgap semiconductor ZnO," Opt. Express **26**, 21364 (2018).
[21]T. Umebayashi, T. Yamaki, H. Itoh, and K. Asai, "Band gap narrowing of titanium dioxide by sulfur doping," Appl. Phys. Lett. **81**, 454 (2002).
[22]N. Kamarulzaman, M. F. Kasim, and N. F. Chayed, "Elucidation of the highest valence band and lowest conduction band shifts using XPS for ZnO and $Zn_{0.99}Cu_{0.01}O$ band gap changes," Results Phys. **6**, 217 (2016).
[23]D. Auvergne, J. Camassel, and H. Mathieu, "Band-gap shrinkage of semiconductors," Phys. Rev. B **11**, 2251 (1975).
[24]H. J. Queisser and E. E. Haller, "Defects in semiconductors: Some fatal, some vital," Science **281**, 945 (1998).
[25]F. Oba and Y. Kumagai, "Design and exploration of semiconductors from first principles: A review of recent advances," Appl. Phys. Express **11**, 060101 (2018).
[26]C. Di Valentin and G. Pacchioni, "Spectroscopic properties of doped and defective semiconducting oxides from hybrid density functional calculations," Acc. Chem. Res. **47**, 3233 (2014).
[27]B. Henderson and G. F. Imbusch, *Optical Spectroscopy of Inorganic Solids* (Oxford University Press, 1989), Vol. 23, p. 2824.
[28]A. V. Chadwick and M. Terenzi, *Defects in Solids: Modern Techniques* (Springer Science & Business Media, 2013), Vol. 23, p. 2824.
[29]M. S. Mrudul, N. Tancogne-Dejean, A. Rubio, and G. Dixit, "High-harmonic generation from spin-polarised defects in solids," npj Comput. Mater. **6**, 10 (2020).
[30]T. Huang, X. Zhu, L. Li, X. Liu, P. Lan, and P. Lu, "High-order-harmonic generation of a doped semiconductor," Phys. Rev. A **96**, 043425 (2017).
[31]C. Yu, K. K. Hansen, and L. B. Madsen, "Enhanced high-order harmonic generation in donor-doped band-gap materials," Phys. Rev. A **99**, 013435 (2019).
[32]X.-F. Pan, T. Han, C.-L. Xia, T.-T. Xu, J. Zhang, and X.-S. Liu, "Energy band splitting and high-order harmonic generation from a doped semiconductor," Laser Phys. Lett. **16**, 115301 (2019).
[33]H. Iravani, K. K. Hansen, and L. B. Madsen, "Effects of vacancies on high-order harmonic generation in a linear chain with band gap," Phys. Rev. Res. **2**, 013204 (2020).
[34]M. O. Henry, J. P. Larkin, and G. F. Imbusch, "Nature of the broadband luminescence center in $MgO:Cr^{3+}$," Phys. Rev. B **13**, 1893 (1976).
[35]J. B. Wachtman and A. D. E. Franklin, "Mass transport in oxides," in Proceedings of a Symposium, Gaithersburg, Maryland, October 22–25, 1967 (1968), Vol. 13, p. 12.
[36]F. Stavale, N. Nilius, and H.-J. Freund, "Cathodoluminescence of near-surface centres in Cr-doped MgO(001) thin films probed by scanning tunnelling microscopy," New J. Phys. **14**, 033006 (2012).
[37]E. Shablonin, A. I. Popov, A. Lushchik, A. Kotlov, and S. Dolgova, "Excitation of different chromium centres by synchrotron radiation in MgO:Cr single crystals," Physica B **477**, 133 (2015).
[38]J. Aramburu, P. García-Fernández, M. Barriuso, and M. Moreno, "Transition metal complexes coupled to vacancies in oxides: Origin of different properties of Cr^{3+} in MgO bounded to a $<100>$ or $<110>$ Mg^{2+} vacancy," J. Phys. Chem. A **117**, 12642 (2013).
[39]J. Aramburu, P. Garcia-Fernandez, J. Garcia-Lastra, M. Barriuso, and M. Moreno, "Colour due to Cr^{3+} ions in oxides: A study of the model system $MgO:Cr^{3+}$," J. Phys. **25**, 175501 (2013).
[40]M. Novita and K. Ogasawara, "Study on multiplet energies of V^{2+}, Cr^{3+}, and Mn^{4+} in MgO host crystal based on first-principles calculations with consideration of lattice relaxation," J. Phys. Soc. Jpn. **83**, 124707 (2014).
[41]J. L. Krause, K. J. Schafer, and K. C. Kulander, "High-order harmonic generation from atoms and ions in the high intensity regime," Phys. Rev. Lett. **68**, 3535 (1992).
[42]P. B. Corkum, "Plasma perspective on strong field multiphoton ionization," Phys. Rev. Lett. **71**, 1994 (1993).
[43]K. C. Kulander, K. J. Schafer, and J. L. Krause, "Dynamics of short-pulse excitation, ionization and harmonic conversion," in *Super-Intense Laser-Atom Physics*, NATO ASI Series (Series B: Physics), Vol. 316, edited by B. Piraux, A. L'Huillier, and K. Rzążewski (Springer, Boston, MA, 1993).
[44]L. V. Keldysh, "Ionization in the field of a strong electromagnetic wave," Sov. Phys. JETP **20**, 1307 (1965).
[45]M. Lewenstein, P. Balcou, M. Y. Ivanov, A. L'Huillier, and P. B. Corkum, "Theory of high-harmonic generation by low-frequency laser fields," Phys. Rev. A **49**, 2117 (1994).
[46]R. Wong, *Asymptotic Approximations of Integrals*, Classics in Applied Mathematics Vol. 34 (Society of Industrial and Applied Mathematics, 2001).
[47]F. Navarrete, M. F. Ciappina, and U. Thumm, "Crystal-momentum-resolved contributions to high-order harmonic generation in solids," Phys. Rev. A **100**, 033405 (2019).
[48]F. Navarrete and U. Thumm, "Two-color-driven enhanced high-order harmonic generation in solids," Phys. Rev. A **102**, 063123 (2020).
[49]L. Kasmi, M. Lucchini, L. Castiglioni, P. Kliuiev, J. Osterwalder, M. Hengsberger, L. Gallmann, P. Krüger, and U. Keller, "Effective mass effect in attosecond electron transport," Optica **4**, 1492 (2017).
[50]M. J. Ambrosio and U. Thumm, "Spatiotemporal analysis of a final-state shape resonance in interferometric photoemission from Cu(111) surfaces," Phys. Rev. A **100**, 043412 (2019).
[51]P. V. C. Medeiros, S. Stafström, and J. Björk, "Effects of extrinsic and intrinsic perturbations on the electronic structure of graphene: Retaining an effective primitive cell band structure by band unfolding," Phys. Rev. B **89**, 041407 (2014).
[52]M. Hjort and S. Stafström, "Modeling vacancies in graphite via the Hückel method," Phys. Rev. B **61**, 14089 (2000).
[53]C. Kittel, *Quantum Theory of Solids* (Wiley, 1987).
[54]A. J. Uzan, G. Orenstein, A. Jiménez-Galán, C. McDonald, R. E. F. Silva, B. D. Bruner, N. D. Klimkin, V. Blanchet, T. Arusi-Parpar, M. Krüger, A. N. Rubtsov, O. Smirnova, M. Ivanov, B. Yan, T. Brabec, and N. Dudovich, "Attosecond spectral singularities in solid-state high-harmonic generation," Nat. Photonics **14**, 183 (2020).
[55]Y. S. You, M. Wu, Y. Yin, A. Chew, X. Ren, S. Gholam-Mirzaei, D. A. Browne, M. Chini, Z. Chang, K. J. Schafer, M. B. Gaarde, and S. Ghimire, "Laser waveform control of extreme ultraviolet high harmonics from solids," Opt. Lett. **42**, 1816 (2017).
[56]G. Vampa, Y. S. You, H. Liu, S. Ghimire, and D. A. Reis, "Observation of backward high-harmonic emission from solids," Opt. Express **26**, 12210 (2018).
[57]A. Miller and D. Finlayson, *Laser Sources and Applications* (CRC Press, 1997), p. 315.
[58]M. Lai, J. Nicholson, and W. Rudolph, "Multiple pulse operation of a femtosecond Ti: sapphire laser," Opt. Commun. **142**, 45 (1997).

[59]J. Philip, C. D'Amico, G. Cheriaux, A. Couairon, B. Prade, and A. Mysyrowicz, "Amplification of femtosecond laser filaments in Ti:sapphire," Phys. Rev. Lett. **95**, 163901 (2005).
[60]Y. Guo, S. Lu, L. Su, C. Zhao, H. Zhang, and S. Wen, "Z-scan measurement of the nonlinear refractive index of Nd^{3+}, Y^{3+}-codoped CaF_2 and SrF_2 crystals," Appl. Opt. **54**, 953 (2015).
[61]S. C. Rae, "Spectral blueshifting and spatial defocusing of intense laser pulses in dense gases," Opt. Commun. **104**, 330 (1994).
[62]A. Heins, S. C. Singh, and C. Guo, "Electron kinetic energy and plasma emission diagnosis from femtosecond laser produced air plasmas," Phys. Plasmas **24**, 072101 (2017).
[63]V. E. Nefedova, M. F. Ciappina, O. Finke, M. Albrecht, J. Vábek, M. Kozlová, N. Suárez, E. Pisanty, M. Lewenstein, and J. Nejdl, "Determination of the spectral variation origin in high-order harmonic generation in noble gases," Phys. Rev. A **98**, 033414 (2018).
[64]Y. S. You, D. Reis, and S. Ghimire, "Anisotropic high-harmonic generation in bulk crystals," Nat. Phys. **13**, 345 (2017).
[65]M. Wu, S. Ghimire, D. A. Reis, K. J. Schafer, and M. B. Gaarde, "High-harmonic generation from Bloch electrons in solids," Phys. Rev. A **91**, 043839 (2015).
[66]X. Liu, X. Zhu, P. Lan, X. Zhang, D. Wang, Q. Zhang, and P. Lu, "Time-dependent population imaging for high-order-harmonic generation in solids," Phys. Rev. A **95**, 063419 (2017).
[67]A. Pattanayak, M. M. S , and G. Dixit, "Influence of vacancy defects in solid high-order harmonic generation," Phys. Rev. A **101**, 013404 (2020).
[68]S. Almalki, A. M. Parks, G. Bart, P. B. Corkum, T. Brabec, and C. R. McDonald, "High harmonic generation tomography of impurities in solids: Conceptual analysis," Phys. Rev. B **98**, 144307 (2018).
[69]Q. Liao, W. Cao, Q. Zhang, K. Liu, F. Wang, P. Lu, and U. Thumm, "Distinction of electron dispersion in time-resolved photoemission spectroscopy," Phys. Rev. Lett. **125**, 043201 (2020).